

Roadside Monocular 3D Detection via 2D Detection Prompting

Yechi Ma¹², Shuoquan Wei², Churun Zhang², Wei Hua², Yanan Li², Shu Kong³⁴

¹Zhejiang University, ²Zhejiang Lab, ³University of Macau, ⁴Texas A&M University

Abstract. The problem of roadside monocular 3D detection requires detecting objects of interested classes in a 2D RGB frame and predicting their 3D information such as locations in bird’s-eye-view (BEV). It has broad applications in traffic control, vehicle-vehicle communication, and vehicle-infrastructure cooperative perception. To approach this problem, we present a novel and simple method by prompting the 3D detector using 2D detections. Our method builds on a key insight that, compared with 3D detectors, a 2D detector is much easier to train and performs significantly better w.r.t detections on the 2D image plane. That said, one can exploit 2D detections of a well-trained 2D detector as prompts to a 3D detector, being trained in a way of inflating such 2D detections to 3D towards 3D detection. To construct better prompts using the 2D detector, we explore three techniques: (a) concatenating both 2D and 3D detectors’ features, (b) attentively fusing 2D and 3D detectors’ features, and (c) encoding predicted 2D boxes’ $\{x, y, \text{width}, \text{height}, \text{label}\}$ and attentively fusing such with the 3D detector’s features. Surprisingly, the third performs the best. Moreover, we present a yaw tuning tactic and a class-grouping strategy that merges classes based on their functionality; these techniques improve 3D detection performance further. Comprehensive ablation studies and extensive experiments demonstrate that our method resoundingly outperforms prior works, achieving the state-of-the-art on two large-scale roadside 3D detection benchmarks.

1 Introduction

Roadside 3D detection is an emerging research problem [56, 58] that has broad applications, e.g., vehicle-vehicle communication [10, 19], vehicle-infrastructure cooperative perception [1], intelligent traffic control [36, 48], etc. A practical yet challenging setup is to use a single RGB camera for roadside perception, known as *roadside monocular 3D detection* [55], which takes an RGB frame as input and aims to detect objects of predefined classes (e.g., vehicle and pedestrian) with 3D information (e.g., depth, 3D shape, orientation, 3D coordinates, etc.).

Status quo. Roadside monocular 3D detection is an ill-posed problem because it requires inferring 3D information from 2D cues alone. Perhaps fortunately, camera pose is fixed on roadside infrastructure, making it possible to train (deep neural) models on massive annotated data to learn to infer such 3D information from a 2D image. To foster the research of roadside monocular 3D detection, the literature has released two large-scale benchmark datasets recently, namely DAIR-V2X-I [58] and Rope3D [56]. Existing methods train sophisticated neural networks in an end-to-end fashion [20, 21]. For 3D detection, a well-known difficulty is precisely estimating depth for objects [14,

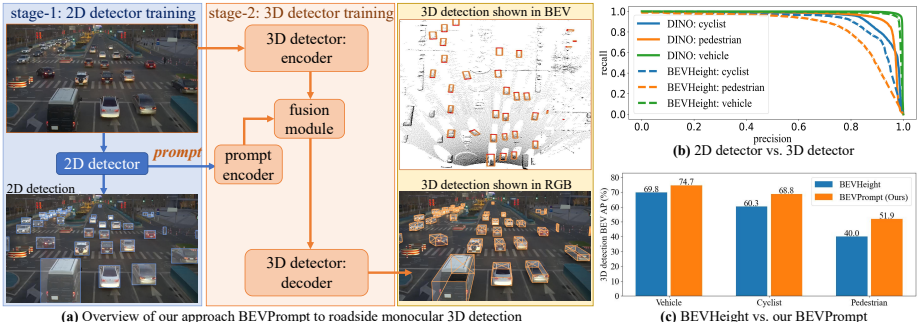


Fig. 1: (a) To approach roadside monocular 3D detection, we introduce BEVPrompt, which first trains a 2D detector and then exploits it to train the monocular 3D detector, which has two crucial modules: *prompt encoder* and *fusion module*. (b) The design choice is motivated by the observation that a simple 2D detector resoundingly outperforms the state-of-the-art 3D detector BEVHeight [55] w.r.t 2D detection metrics, as shown by the results on the DAIR-V2X-I dataset. This implies that 2D detection is an “easier” task than monocular 3D detection, although we use the same dataset to train detectors. In particular, to exploit the 2D detector to facilitate 3D detector training, we study how to use 2D detections as prompts and attentively fusing them with 3D detector’s feature (details in Fig. 2). (c) Our BEVPrompt significantly outperforms the state-of-the-art method BEVHeight across semantic classes (cf. more quantitative results in Table 1).

40, 52]. To mitigate this difficulty in the context of roadside monocular 3D detection, [55] proposes BEVHeight that converts the problem of depth estimation to object height estimation and exploits camera parameters to infer object depth, achieving the state-of-the-art performance.

Motivation. While BEVHeight [55] achieves the state-of-the-art performance for roadside monocular 3D detection, perhaps surprisingly, we find that it *underperforms* 2D detectors (e.g., DINO [59]) measured by 2D detection metrics, as shown by the precision-recall curves on the DAIR-V2X-I dataset [58] in Fig. 1b. Note that, to train the 2D detector DINO [59] on this dataset, we project 3D cuboid annotations onto the image plane to derive 2D box annotations and use such for training. To evaluate BEVHeight w.r.t 2D detection metrics, we project its 3D detections onto the 2D image plane. Admittedly, this comparison is somewhat unfair because DINO and BEVHeight have different network architectures, but it has several important implications: (1) 2D detection is a much “easier” task than monocular 3D detection, (2) 2D detectors are “easier” to train than 3D detectors, (3) 2D detectors are better understood and their techniques are better explored, etc. This comparison motivates us to *improve roadside monocular 3D detection by exploiting a 2D detector*.

Technical insights. Training a 3D detector involves optimizing multiple objectives, such as 2D box coordinate regression, depth estimation, orientation regression, and object classification. Intuitively, a compound holistic objective that optimizing all together might cause the missing detection of some hard objects as an attempt to handle the difficulty in regressing coordinates, depth and orientation. In contrast, training a 2D detector is simpler that incorporates fewer loss terms (e.g., only a 2D box coordinate regression loss and a classification loss) and is well studied in the literature. As a re-

sult, a 2D detector outperforms the 3D detector (although they are trained on the same dataset) w.r.t 2D detection metrics, motivating our exploration of using a 2D detector to facilitate 3D detector training. Moreover, there are more publicly available datasets with 2D box annotations, allowing pretraining a stronger base 2D detector and finetuning it on the target roadside dataset towards better performance. We study how to effectively use what is learned in the 2D detector to improve 3D detection. First and foremost, we explore using 2D detections as *prompts*¹ to help train better 3D detectors (Fig. 1a). A straightforward method is to concatenate the *features* computed by the 2D detector with the 3D detector’s features, which notably improves the 3D detection performance. Another approach is to attentively fuse these *features*, inspired by recent transformer architectures or attention modules, which exhibits markedly superior performance to the simple concatenation (Table 5). Nevertheless, we derive a rather simple and effective method that uses 2D *detection output* as prompts (i.e., 2D boxes’ coordinates and class labels) to attentively fuse 3D detector’s features, leading to significant improvements (Fig. 1c). Intuitively, this attributes to that using 2D detections gives pinpointed targets, based on which training the 3D detector boils down to a simpler problem of inflating 2D detections to BEV. Moreover, we use the 2D detections to optimize rotation prediction of the 3D detections. Concretely, we introduce a yaw-tuning technique that optimizes rotation of a 3D detection w.r.t the corresponding 2D box prediction. This improves 3D detection further.

Technical contributions. We reiterate our technical contribution as the proposed BEVPrompt method (Fig. 1a), which uses a 2D detector to facilitate the training of the 3D detector. We study multiple approaches to exploit the 2D detector by using either its features or detection output as prompts. Our final method uses the 2D detection output, a 5-dim vector $\{x, y, \text{width}, \text{height}, \text{label}\}$, as the prompt, encodes it and attentively fuses it with features of the 3D detector being trained. Moreover, we present a class-grouping strategy to train multiple heads in the 3D detector and a yaw tuning tactic to refine orientation predictions, leading to further improvement. Comprehensive ablation studies and extensive experiments demonstrate that our BEVPrompt resoundingly outperforms prior work on two recent large-scale benchmark datasets.

2 Related Work

Roadside monocular 3D detection is proposed to help autonomous driving. The motivation is that autonomous vehicles have limited range of perception [14], but a camera hung on a high infrastructure provides perception in a longer range [55]. Through vehicle-infrastructure cooperative perception, vehicles can drive more safely. In addition, roadside monocular 3D detection can also help unexpected events detection and traffic congestion prediction. To foster research of 3D object detection on roadside scenes, the community recently established two large-scale datasets, namely DAIR-V2X-I [58] and Rope3D [56]. Moreover, among existing approaches to roadside 3D monocular detection, BEVHeight [55] achieves the state-of-the-art performance on the

¹ We use “prompt” to emphasize that the information used to help train 3D detectors is provided by the 2D detector, which is frozen during training 3D detectors.

two datasets. It trains a model to regress towards objects height instead of object distance or depth, as done previously [20]. It finds that regressing height is an easier task than regressing depth given the fixed camera pose. Our work recognizes that a fruitful space to improve over BEVHeight is to train a 2D detector (Fig. 1b) using 2D box annotations derived by projecting the 3D annotations on the image plane and then to exploit the 2D detector to facilitate 3D detector training (Fig. 1a). We show that our method significantly outperforms BEVHeight (Fig. 1c) on the two well-established datasets.

2D object detection is a fundamental computer vision problem [11, 22], requiring detecting all objects belonging to some predefined categories. Prevailing approaches train deep neural networks for 2D detection. The mainstream detector architecture consists of a backbone to encode input images, and a detector-head for box regression and classification [25, 37, 38, 45]. Recent developments in transformer architectures improve 2D object detection significantly further [8, 59, 62]. We explore how to leverage a 2D detector to train better monocular 3D detectors on roadside scenes. We exploit the state-of-the-art 2D detector DINO [59] and YOLOV7 [45] in this work. It is important to note that any 2D detectors can be used in our framework. To the best of our knowledge, we make the first attempt to explicitly exploit a 2D detector to improve roadside monocular 3D detection.

Joint training versus stage-wise training. Both training paradigms exist in the literature. For 3D detection, various methods jointly train the 3D detector and a 2D detector by incorporating 2D annotations in an auxiliary loss [13, 20, 27, 33, 42, 46, 47, 60]. BEVFormer v2 [54] trains a 3D detector jointly using two 3D losses in BEV and perspective views. [30, 50] also jointly train detectors to dynamically generate (2D) queries for input images and use such for 3D output. Stage-wise training is also widely adopted in various methods. For example, [38] trains a proposal detector first and then a detector head for box regression and classification. [16] trains a planner in multiple stages, i.e., training individual modules (e.g., for tracking, mapping, motion forecasting, etc.) in separate stages. We examine both paradigms for our monocular 3D detector training that exploits a 2D detector, and find that stage-wise training remarkably outperforms joint training.

Prompting, enabled by large language models (LLMs), is first recognized in Natural Language Processing (NLP) [6, 41, 51]. Briefly, given a generative LLM, using a text prompt can instruct the model to produce desired text outputs. Inspired by this, the computer vision community endeavors to train large visual/multimodal models that can take text prompts to generate, restore and edit images [26, 32, 35]. Some works use images as prompts to accomplish vision tasks such as segmentation and inpainting [2, 49]. Beyond visual and text prompts, some recent works use more diverse information as prompts to guide models to produce desired output. For example, the Segment Anything Model (SAM) accepts bounding boxes, segmentation masks, and foreground/background points as prompts towards interactive segmentation [17]. Inspired by above, we train a 3D detector that accepts prompts given by a well-trained 2D detector. The prompt can be as simple as predicted 2D coordinates and labels, similar to what used in SAM. Our method of using 2D detections as prompts significantly improves 3D detection performance (Fig. 1c, Table 1).

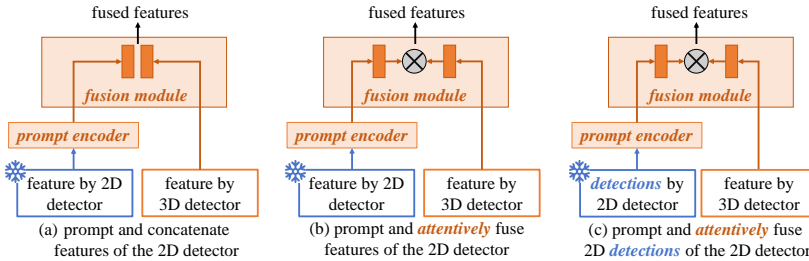


Fig.2: We study three designs of *prompt encoder* and *fusion module* (Fig. 1a), used to exploit the 2D detector to facilitate 3D detector training. Design (a) concatenates feature maps extracted by the 2D detector and the 3D detector encoder. Design (b) extracts a feature vector based on a 2D detection’s coordinates, encodes it through a *prompt encoder* (implemented as a MLP), and attentively fuses it with the feature map extracted by the 3D detector’s encoder. The fusion is done in the *fusion module* (implemented by a transformer building block). Design (c) encodes a 2D detection, a 5-dim vector (coordinates x and y , object width w and height h , predicted class label) as the prompt, and attentively fuses the encoded feature with the feature map of the 3D detector encoder through the fusion module.

3 Methods

We first present the problem of roadside monocular 3D object detection, then introduce our approach, its important modules along with design choices, and novel techniques for further improvements.

Problem definition. Roadside monocular 3D detection requires detecting objects from a 2D RGB image and predicting their 3D information including (x, y, z, w, h, l, yaw) , where (x, y, z) is the object’s center location in the 3D world, (w, h, l) denotes the width, height and length of the cuboid capturing the 3D object, and yaw denotes the orientation of the cuboid on the BEV plane.

3.1 The proposed method: BEVPrompt

Our BEVPrompt exploits a well-trained 2D detector to improve 3D detection (Fig. 1a). We first train a 2D detector using the training set that consists of monocular images and 2D box annotations on the objects of interest. While the datasets might only contain 3D cuboid annotations, we derive the 2D box annotations using the camera extrinsic and intrinsic parameters to project the 3D cuboid annotations onto the 2D image plane towards 2D box annotations. After training the 2D detector, we freeze and use it to extract either features or 2D detections, which are used as *prompt* for the 3D detector being trained later. The architecture of the 3D detector contains a visual encoder to encode input images, a decoder to make 3D predictions, and importantly, two novel modules in between: *prompt encoder* and *fusion module*. The *prompt encoder* encodes the prompt into features, and the *fusion module* incorporates them before the decoder for 3D detection. We elaborate the two modules below.

Prompt encoder transforms features or 2D boxes provided by the 2D detector into new features, which are then exploited for 3D detections. The prompt encoder can be implemented as either a set of convolutional layers or a multi-layer perceptron (MLP)

depending on what are used as prompts and how to fuse (explained in the *fusion module* below). For example, if feature maps of the 2D detector are used as prompts, then the prompt encoder can be a set of convolutional layers with non-linear transforms (e.g., ReLU) that encode feature maps into new feature maps at appropriate dimensions (Fig. 2a). This ensures that the new feature maps can be fused with those of the 3D detector’s encoder through the *fusion module*. In our work, we consider using three different types of information as prompts: (1) feature maps represented as tensors, (2) feature vectors at the spatial position specified by the predicted coordinates of 2D detections, and (3) the 2D detection output (e.g., box coordinates x and y , width, height, and class label). Somewhat surprisingly, (3) performs the best (Table 5)! To be specific, to encode a 2D detection output, we represent a predicted 2D box with a normalized positional encoding of its top-left and bottom-right corners, and represent the class label as a class index ID. We learn an MLP to transform them into a feature vector, using which to attentively fuse a feature map of the 3D detector (cf. details in supplement).

Fusion module fuses the feature prompts (from the prompt encoder) and feature maps of the 3D detector’s encoder (Fig. 2). If the feature prompts are feature maps, then a straightforward fusion method is to concatenate them (Fig. 2a), as widely adopted in the literature [28, 34]. Inspired by the recent transformer architecture [44] and its application in prompt encoding [17], we propose to use an attention module to fuse these features. Experiments demonstrate that such attentive fusion outperforms concatenation (Table 5). Concretely, we denote the feature map from the encoder F in the 3D detector for an input image X as $F(X)$; the prompt encoder F_{prompt} transforms the input prompts p into vectors $F_{prompt}(p)$. The fusion model returns the final fused feature $f = \text{Transformer}(F(X), F_{prompt}(p))$. Briefly, the *Transformer* processes features in three steps (detailed in the supplement): (1) applying self-attention on the feature prompts $F_{prompt}(p)$, producing a new feature f_1 ; (2) applying cross-attention between f_1 as query and $F(X)$, followed by an MLP that produces feature f_2 ; (3) applying cross-attention between $F(X)$ as query and f_2 , producing the final fused feature f .

3.2 Remarks

Our method BEVPrompt exploits a 2D detector for 3D detection (Fig. 1a). In principle, our method can use any 2D detectors. We make three remarks below.

Techniques of 2D detection are well established. In object detection, 2D detection is better explored than monocular 3D detection, primarily due to historical reasons that the former has been a fundamental problem in computer vision whereas the latter is relatively new. There are many excellent 2D detectors developed in the past years along with the developments of CNNs and transformers, such as FasterRCNN [38], YOLO [3, 45], DETR [9] and DINO [59]. In the benchmarking results, we use the transformer-based detector DINO [59], which achieves the state-of-the-art performance on various 2D detection benchmark datasets. In the ablation studies, we use other 2D detectors.

More datasets of 2D detection are publicly available. As 2D detection is a fundamental problem in computer vision and has been actively explored since the past decade, many large-scale datasets have been released to the public. In contrast, for the relatively new problem of monocular 3D detection, there are less datasets which are also small in scale compared to the 2D counterpart. For example, the 2D detection dataset

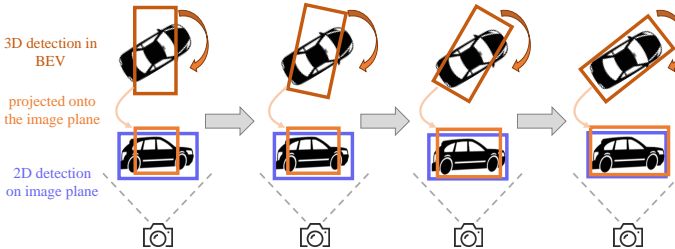


Fig. 3: Yaw tuning optimizes the orientation of 3D detection in BEV with the objective to maximize the IoU between the projected 3D detection and the corresponding 2D detection box.

COCO [23] (published in 2014) annotates 330K images with 2D boxes for 80 classes, whereas the 3D detection dataset nuScenes [7] (published in 2020) “only” annotates 144K RGB images with 3D cuboids for 23 classes. Moreover, labeling 3D cuboids often relies on other sensors (e.g., LiDAR) so to obtain 3D information (e.g., depth) for 3D annotation. Nevertheless, existing 2D datasets enable pretraining a strong 2D detector, finetuning which on the roadside dataset improves 3D detector training (Fig. 5).

Stage-wise training outshines joint training. We find that stage-wise training a 2D detector followed by 3D detector training outperforms jointly training a 3D detector (cf. Table 1). We attribute the advantage of stage-wise training to two reasons. First, 2D detector training is better explored with mature techniques than 3D detector training, so stage-wise training makes use of mature techniques of 2D detector training. Second, joint training must strike a balance between various loss functions such as 3D cuboid regression, rotation regression and so on; yet optimizing over all losses inevitably sacrifices 2D detection which is actually much easier than 3D detection. It is worth noting that stage-wise training allows easily leveraging external 2D datasets for pretraining a much better 2D detector. Starting with such a pretrained 2D detector significantly improves 3D detection (cf. Fig. 5).

3.3 Further Improvement by Tuning Yaw

In 3D detection, correctly predicting the yaw (i.e., the orientation on the BEV plane) of objects is crucial to various downstream tasks. We observe that, when we project 3D cuboids (predicted by the 3D detector) onto the 2D image plane, they usually misalign with the 2D boxes predicted by the 2D detector. Considering that the 2D detector performs sufficiently well w.r.t 2D detection metrics, we are inspired to optimize the predicted yaw for each 3D detection using the corresponding 2D box detection by the 2D detector. Specifically, we rotate a 3D cuboid along the yaw axis to maximize the IoU of its 2D projected box with the corresponding 2D box by the 2D detector. Fig. 3 illustrates how to tune yaw. Fig. 6 shows visual comparisons between with and without yaw tuning and Table 7 lists quantitative comparisons, validating the effective of our yaw-tuning technique.

3.4 Class Grouping and Multi-Head Design

Class grouping is a common strategy in 3D object detection. It merges classes into some superclasses, allowing trained features to be shared within superclasses [61]. Moreover, multi-head design follows along with groups of classes for discriminative



Fig.4: Visual comparison between the state-of-the-art method BEVHeight [55] and our BEVPrompt. Results show that our BEVPrompt can (1) make better orientation predictions than BEVHeight (column-1), and (2) detect objects (missed by BEVHeight) that are too small in size (column-2), heavily occluded (column-3), and in long distance (column-4).

predictions across fine-grained classes [57]. BEVHeight [55] adopts class grouping and multi-head design by considering the similarities among object appearance, e.g., size and shape in the 3D world. For example, on DAIR-V2X-I, BEVHeight creates three superclasses that merge $\{truck, bus\}$, $\{car, van\}$, and $\{bicyclist, tricyclist, motorcyclist, barrowlist\}$, respectively, along with the origin *pedestrian* class. It learns a four-head detector with each making predictions for the corresponding superclass (cf. details in supplement). We call this grouping strategy *appearance-based grouping*. Differently, we adopt *functionality-based grouping*, i.e., merging $\{car, van, truck, bus\}$ into *vehicle*, and $\{bicyclist, tricyclist, motorcyclist, barrowlist\}$ into *cyclist*. This is motivated by the fact that vehicles, cyclists and pedestrians appear at relatively fixed regions on the roadside images. We expect this grouping strategy, or using the location prior of different classes, to facilitate training 3D object detectors on roadside images. Perhaps from the same functionality perspective, the DAIR-V2X-I benchmark also merges classes into such superclasses for evaluation. Our extensive study shows that the functionality-based grouping strategy remarkably improves detection performance (Table 6).

4 Experiments

We validate our method BEVPrompt and design choices through extensive experiments. First, we present experimental settings including two benchmark datasets, evaluation metrics and important implementations details. Then, we compare our BEVPrompt against prior work including BEVHeight [55] which has achieved the best numbers on the benchmarks. Lastly, we present rigorous ablation studies for our method. We will open-source our code which is a part of our supplementary material.

4.1 Experimental Settings

Datasets. We use DAIR-V2X-I [58] and Rope3D [56] in experiments. Both datasets are publicly available for academic purposes. They contain LiDAR data but the problem of monocular 3D detection does not use it (we use LiDAR for visualization in this work). LiDAR can be thought of as a tool for 3D annotation and visualization.

- DAIR-V2X-I is the first large-scale dataset supporting the research of roadside monocular 3D detection. It has 5K training images and 2K validation images.

Table 1: Benchmarking results on the DAIR-V2X-I dataset. Following [55], we report AP metrics at IoU=0.5, 0.25, 0.25 in BEV for the three superclasses (Vehicle, Cyclist, and Pedestrian), respectively. We mark the modalities (M) used in each method: C for RGB camera, L for LiDAR. As our BEVPrompt can be a plugin to other methods, we apply it to BEVDepth and BEVHeight. Results show that incorporating BEVPrompt significantly improves these methods. Notably, our BEVPrompt improves the original BEVHeight by >10 AP on Pedestrian! This attributes to the 2D detector which detects pedestrians much better than the 3D detector BEVHeight, as verified in Fig. 1b. Table 4 analyzes different architectural designs of BEVPrompt.

Method	M	Vehicle			Cyclist			Pedestrian		
		Easy	Mid	Hard	Easy	Mid	Hard	Easy	Mid	Hard
PointPillars [18]	L	63.1	54.0	54.0	38.5	22.6	22.5	38.5	37.2	37.3
SECOND [53]	L	71.5	54.0	54.0	54.7	31.1	31.2	55.2	52.5	52.5
MVXNet [43]	L+C	71.0	53.7	53.8	54.1	30.8	31.1	55.8	54.5	54.4
ImvoxelNet [39]	C	44.8	37.6	37.6	21.1	13.6	13.2	6.8	6.7	6.7
MV2D [50]	C	57.6	46.3	46.4	21.7	21.6	21.6	15.5	14.6	14.9
BEVFormer [21]	C	61.4	50.7	50.7	22.2	22.1	22.1	16.9	15.8	16.0
BEVFormer v2 [54]	C	62.9	52.3	52.3	25.3	25.2	25.2	18.0	17.1	17.2
SparseBEV [24]	C	65.6	55.1	52.6	30.0	30.3	30.0	18.4	17.9	17.5
BEVDepth [20]	C	75.5	63.6	63.7	55.7	55.5	55.3	35.0	33.4	33.3
+ BEVPrompt	C	78.4	70.7	70.6	58.5	58.4	58.3	42.7	42.1	42.3
BEVHeight [55]	C	77.8	65.8	65.9	60.2	60.1	60.5	41.2	39.3	39.5
+ BEVPrompt	C	83.3	71.4	71.8	68.1	70.8	71.0	53.6	52.4	51.9

Following [55], we report benchmarking results on the validation set, with breakdown analysis w.r.t three superclasses, “vehicle”, “cyclist”, and “pedestrian”, at three difficulty levels (Easy, Medium, Hard).

- Rope3D is another large-scale dataset that contains 50k images and annotates over 1.5M 3D objects in various scenes. Following [55], we use its training set (70%) to train models and the validation set (30%) to report benchmarking results.

Metrics. Below, we introduce several metrics to sufficiently benchmark methods.

- $AP_{IoU=t}$ is the (average) precision (AP) at IoU threshold t on the BEV plane. To benchmark methods on DAIR-V2X-I (i.e., in Table 1), we follow [55] which sets $t = 0.25$ when evaluating on cyclist and pedestrian classes, and $t = 0.5$ on vehicle class. To highlight performance improvement in ablation studies (cf. Table 5-8 and Fig. 5, we set $t = 0.5, 0.5, 0.7$ for the aforementioned classes, respectively).
- To report 2D detection performance on the image plane (cf. Table 3 and Fig. 5) we use mean AP (mAP) [23]. It first computes per-class precision averaged (AP) at IoU thresholds from 0.5 to 0.95 with a step-size 0.05 and returns the mean of per-class APs.
- On the Rope3D benchmark dataset [56], we report numbers w.r.t its official metrics of $AP_{IoU=t}$ in BEV [42] and $Rope_{score}$. The latter is a sophisticated metric that jointly considers detection errors of orientation, area, and BEV box coordinates compared to the ground-truth.
- To analyze our yaw-tuning technique, we further use the $AOS_{IoU=t}$ metric, which measures the average orientation similarity (AOS) at IoU threshold t [12].

Implementations. 3D detectors studied in our work mostly follow BEVHeight [55], which contains an image encoder with ResNet101 architecture [15], a BEV encoder with ResNet18 architecture, an FPN for proposal detection [53], and a detector head

Table 2: Benchmarking results on the Rope3D dataset. Following [56], we use metrics AP and Rope at IoU=0.5 and 0.7. Built on BEVHeight, BEVPrompt achieves significant improvement. Conclusions drawn in Table 1 hold on this dataset.

Method	IoU = 0.5				IoU = 0.7			
	Car		Big Vehicle		Car		Big Vehicle	
	AP	Rope	AP	Rope	AP	Rope	AP	Rope
M3D-RPN [4]	54.2	62.7	33.1	44.9	16.8	32.9	6.9	24.2
Kinematic3D [5]	50.6	58.9	37.6	48.1	17.7	32.9	6.1	22.9
MonoDLE [31]	51.7	60.4	40.3	50.1	17.7	32.9	6.1	22.9
MonoFlex [60]	60.3	66.9	37.3	48.0	33.8	36.1	10.1	26.2
BEVFormer [21]	50.6	58.8	34.6	45.2	24.6	38.7	10.1	25.6
SparseBEV [24]	54.7	62.3	39.8	48.4	29.9	41.2	14.6	30.0
BEVDepth [20]	69.6	74.7	45.0	54.6	42.6	53.1	21.5	35.8
BEVHeight [55]	74.6	78.7	48.9	57.7	45.7	55.6	23.1	37.0
+ BEVPrompt	82.2	84.7	73.9	77.4	49.1	58.3	30.7	42.9

Table 3: Comparison of methods’ 2D detection metric (mAP) on DAIR-V2X-I. For both 2D detector (DINO) and 3D detectors BEVDepth and BEVHeight, we train them on the training set of DARI-V2X-I (the 1st row). To evaluate 3D detectors w.r.t 2D metrics, we project their 3D detections onto the 2D image plane to derive their predicted 2D boxes. DINO achieves >10 mAP higher than the prior art BEVHeight on all classes and nearly 20 mAP higher than BEVHeight on the pedestrian class! Owing to better exploiting the 2D detector DINO, our method BEVPrompt significantly outperforms the original BEVDepth and BEVHeight.

Method	Vehicle			Cyclist			Pedestrian		
	Easy	Mid	Hard	Easy	Mid	Hard	Easy	Mid	Hard
2D detector (DINO) [59]	74.3	75.6	75.6	57.3	54.7	54.9	50.6	51.6	51.6
BEVDepth [20]	62.9	64.8	64.2	41.5	44.8	44.9	32.9	33.1	33.0
+ BEVPrompt	68.0	68.3	68.9	45.9	47.7	47.6	42.1	42.6	42.6
BEVHeight [55]	63.5	64.7	64.5	41.4	44.6	44.7	33.6	33.7	33.9
+ BEVPrompt	68.1	68.8	68.8	47.9	49.5	49.4	42.8	43.5	43.5

for the final output of 3D detections. Yet, it is worth noting that our BEVPrompt replaces the ResNet18-based BEV encoder with a single convolutional layer, removes the FPN as it does not require proposal detection anymore (as replaced by the 2D detection prompts). This helps our BEVPrompt to achieve faster inference than BEVHeight (cf. Table 8). We build our BEVPrompt atop of either BEVDepth or BEVHeight, allowing fair comparisons against them. We train DINO [59] with the backbone ViT-S/16 as the 2D detector using the default hyperparameter setting. For all the methods, the input image resolution is 864x1536 and the initial voxel resolution is 1024x1024x1. We use random scaling and rotation augmentation during training, and train all models for 50 epochs (long enough for convergence) using AdamW optimizer [29] with learning rate 8e-4. We select the best checkpoint via validation. In post-processing, we remove detections that have confidence scores lower than 0.3.

4.2 Benchmarking Results

We compare our BEVPrompt against prior works on DAIR-V2X-I (Table 1) and Rope3D (Table 2). Results demonstrate that our method achieves the state-of-the-art, resoundingly outperforming previous ones. Fig. 4 visualizes results by BEVPrompt and

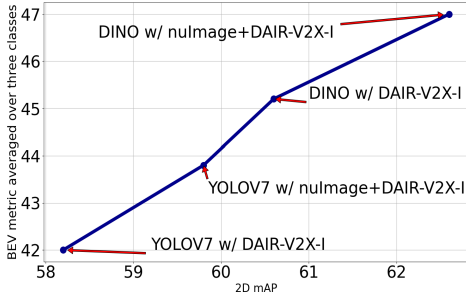


Fig. 5: We train different 2D detectors (YOLOV7 [45] and DINO [59]) on different amounts of 2D annotations (provided by nuImages [7]) for BEVPrompt. We measure the 3D detection by averaging AP over the three classes vehicle, cyclist and pedestrian with thresholds 0.7, 0.5 and 0.5, respectively. Training on more 2D annotations leads to better 2D detectors and importantly, increases 3D detection performance of BEVPrompt.

Table 4: Comparison of stage-wise training vs. joint end-to-end training in our BEVPrompt.

Results are comparable to those in Table 1, i.e., on the same DAIR-V2X-I dataset and using the same metrics. Moreover, we show that not sharing (NS) a visual encoder (marked as NS) for 2D and 3D detectors performs better. In this case, we use ViT-S/16 network for the 2D detector (DINO [59]). This allows us to use more 2D data (marked as MD) from external data source (from nuImages [7]) to pretrain the 2D detector. Results convincingly show that (1) stage-wise training outperforms joint end-to-end training for roadside monocular 3D detection; (2) not sharing backbone offers the flexibility of using different 2D detector architectures and enables training a better 2D detector; (3) exploiting more 2D data also helps train a better 2D detector and in turn improves 3D detector training.

Method	M	Vehicle			Cyclist			Pedestrian		
		Easy	Mid	Hard	Easy	Mid	Hard	Easy	Mid	Hard
BEVDepth [20]	C	75.5	63.6	63.7	55.7	55.5	55.3	35.0	33.4	33.3
+ BEVPrompt: joint	C	76.2	65.3	65.2	56.4	56.5	56.4	38.6	38.1	38.1
+ BEVPrompt: stage-wise	C	76.8	67.4	67.3	56.6	56.7	56.6	39.9	39.5	39.5
+ BEVPrompt: stage-wise, NS	C	77.1	69.2	69.1	57.1	57.0	56.9	41.3	40.0	40.2
+ BEVPrompt: stage-wise, NS, MD	C	78.4	70.7	70.6	58.5	58.4	58.3	42.7	42.1	42.3
BEVHeight [55]	C	77.8	65.8	65.9	60.2	60.1	60.5	41.2	39.3	39.5
+ BEVPrompt: joint	C	79.1	67.4	67.3	62.0	63.9	64.1	47.1	45.9	45.8
+ BEVPrompt: stage-wise	C	81.0	69.3	69.2	64.1	67.6	67.8	49.1	48.4	48.0
+ BEVPrompt: stage-wise, NS	C	82.9	70.6	70.5	66.9	69.6	69.8	52.9	51.9	50.8
+ BEVPrompt: stage-wise, NS, MD	C	83.3	71.4	71.8	68.1	70.8	71.0	53.6	52.4	51.9

BEVHeight (cf. the supplement for more visuals), demonstrating the superiority of our BEVPrompt over improves BEVHeight for roadside 3D monocular detection.

We further compare methods’ performance w.r.t 2D detection metrics (cf. Table 3). This helps us to understand that (1) the 2D detection performance greatly reflects the 3D detection performance; (2) exploiting the 2D detector which yields much better 2D detection performance, our BEVPrompt achieves much better 3D detection performance. In particular, we plot a curve between 2D detection performance (by training different 2D detectors) and 3D detection performance by our BEVPrompt in Fig. 5. Here, we exploit more 2D annotations (from nuImages [7]) to pretrain different 2D detectors (e.g., YOLOV7 [45] and DINO [59]) and finetune on the target dataset DAIR-V2X-I. This helps us to obtain different 2D detectors of different performances. The curve in Fig. 5 clearly shows that exploiting better 2D detectors notably improves 3D detection performance by our BEVPrompt.

Table 5: How to use the 2D detector to prompt the 3D detector. We compare six prompting methods in our BEVPrompt and compare against the prior art BEVHeight. We report results w.r.t AP metric in BEV with IoU thresholds [0.7, 0.5, 0.5] for [vehicle, cyclist and pedestrian]. First, all prompting methods achieve remarkable improvement over BEVHeight. Interestingly, using the center of predicted 2D box coordinates (“fusing 2D centers”) as prompts outperforms feature prompts. Additionally incorporating predicted labels brings further improvements.

Method	Vehicle			Cyclist			Pedestrian		
	Easy	Mid	Hard	Easy	Mid	Hard	Easy	Mid	Hard
BEVHeight	67.4	67.2	67.2	23.6	25.9	26.5	11.5	11.4	11.5
concat feaMaps	73.7	73.3	73.4	29.3	32.1	32.2	14.1	13.9	13.9
fusing vectors	73.8	74.2	74.5	29.4	32.3	32.4	15.0	14.9	14.9
fusing 2D centers	74.0	75.0	74.6	29.6	32.2	32.2	15.5	15.4	15.3
+ 2D labels	74.3	75.3	74.5	30.6	31.4	31.0	16.8	16.7	16.6
fusing 2D boxes	75.1	77.0	73.8	30.1	32.8	33.0	16.3	16.1	16.1
+ 2D labels	75.3	77.2	74.5	32.1	36.1	36.0	17.8	17.7	17.7

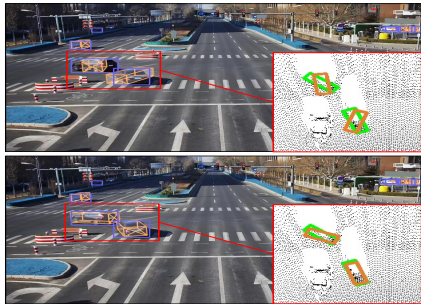


Fig. 6: Visual comparison between without (top) and with (bottom) yaw tuning. Orange boxes are 3D detections by our BEVPrompt. Ground-truth boxes are in green in BEV; 2D box predictions are in blue on the image plane. Tuning yaw clearly improves 3D detection results. Refer to Fig. 7 for quantitative results.

Method	Vehicle w.r.t metrics AP _{IoU=0.7} / AOS		
	Easy	Mid	Hard
BEVHeight	67.4 / 88.5	67.2 / 90.2	67.2 / 90.2
w/o yaw tuning	75.2 / 92.7	77.0 / 94.8	76.8 / 94.8
w/ yaw tuning	75.9 / 95.6	77.6 / 95.3	77.3 / 95.3

Fig. 7: Yaw tuning improves 3D detection.

For the *vehicle* class, we tune the yaw / orientation of 3D detections by exploiting 2D detections. This is motivated that 3D vehicle detections do not necessarily have good orientations. When projected on the image plane, 3D cuboids do not align well with 2D boxes of the 2D detector. We optimize detection orientations by rotating 3D cuboid along the yaw-axis to maximize the IoU between projected 3D rotated cuboid and the corresponding 2D detection box, as illustrated in Fig. 3.

4.3 Ablation Studies

Stage-wise training vs. joint training. In our work, we have tested different training paradigms in our BEVPrompt, e.g., (1) stage-wise training of the 2D detector and then 3D detector, and (2) joint end-to-end training the 3D detector using both 2D and 3D losses. Table 4 compares results of BEVPrompt built on top of BEVDepth and BEVHeight. We refer the reader to the caption therein for salient conclusions.

What to use as prompts. To exploit the 2D detector to help train 3D detectors, we study what information from it can be used as prompts, including its intermediate feature map, feature vector located at a 2D detection, and even the simplistic 2D detection output (i.e., predicted box coordinates and class label). Note that using different things in prompts requires different fusion methods. For example, when using feature maps, one can concatenate them with feature of the encoder in the 3D detector, while using feature vectors or detections output require fusing vectors with the feature maps. Therefore, we use concatenation to fuse feature maps, and an attention module to fuse

Table 6: Ablation on class-grouping strategies (w.r.t metric AP in BEV). Grouping classes differently with multi-head design (each detector head makes predictions within a specific super-class) makes a difference in training and yields detectors performing differently. Briefly, instead of appearance-based grouping (AG) which groups classes w.r.t object appearance as done by BEVHeight, we do functionality-based grouping (FG), e.g., merging {car, van, truck, bus} into the superclass vehicle. To justify the superiority of FG over AG, we replace BEVHeight’s original AG with our FG, particularly improving on the vehicle class (cf. “BEVHeight w/ FG” vs “BEVHeight w/ AG”).

Method	Vehicle			Cyclist			Pedestrian		
	Easy	Mid	Hard	Easy	Mid	Hard	Easy	Mid	Hard
BEVHeight w/ AG	67.4	67.2	67.2	23.6	25.9	26.5	11.5	11.4	11.5
+ BEVPrompt w/ AG	73.3	74.1	72.7	32.0	35.9	35.8	17.7	17.7	17.7
BEVHeight w/ FG	72.0	73.6	72.0	23.5	25.7	26.4	10.1	10.1	10.2
+ BEVPrompt w/ FG	75.3	77.2	74.5	32.1	36.1	36.0	17.8	17.7	17.7

Table 7: How to train BEVPrompt (w.r.t metric AP in BEV). When training the 3D detector by our BEVPrompt, constructing the prompt can use either ground-truth 2D boxes or predicted ones by the pretrained 2D detector. We compare them on DAIR-V2X-I w.r.t AP in BEV. Results show that using 2D box predictions (pred) outperforms ground-truth 2D annotations (grnd).

Method	Vehicle			Cyclist			Pedestrian		
	Easy	Mid	Hard	Easy	Mid	Hard	Easy	Mid	Hard
BEVHeight	67.4	67.2	67.2	23.6	25.9	26.5	11.5	11.4	11.5
+ BEVPrompt w/ grnd	75.3	77.2	74.5	32.1	36.1	36.0	17.8	17.7	17.7
+ BEVPrompt w/ pred	75.2	77.0	76.8	34.1	36.1	36.0	18.9	18.6	18.5

the feature vectors. Table 5 lists the results. Perhaps surprisingly, using the simple detections (2D boxes and class labels) in prompts performs better than feature maps and feature vectors located at 2D detections, where 2D boxes as prompts achieves [73.8, 33.0, 16.1] AP for Hard examples of the three classes [vehicle, cyclist, pedestrian]. Furthermore, additionally incorporating the predicted class labels in prompts performs the best, boosting to [74.5, 36.0, 17.7] AP on Hard examples of the three classes!

Yaw tuning for improvement. Fig. 6 and 7 demonstrate improvements by yaw tuning qualitatively and quantitatively. Results show that yaw tuning notably improves 3D detection performance in terms of not only the average orientation similarity metric (AOS) but also the 3D detection metric (AP).

How to group classes and design the 3D detector head. Section 3.4 details class grouping strategies and multi-head design. BEVHeight adopts an *appearance-based grouping* (AG) [55], e.g., merging big vehicle classes bus and truck together; whereas we propose *functionality-based grouping* (FG), e.g., merging all vehicles together including bus, truck, van, and car. Table 6 compares these methods, showing that the our FG indeed outperforms AG. To justify this further, we train BEVHeight using our FG, leading to remarkable improvements particularly on the vehicle class.

How to train 3D detectors with 2D detection prompts. Our BEVPrompt requires 2D detection prompts to make 3D predictions. To train the 3D detector, we can either use ground-truth 2D boxes or predicted ones as prompts. We compare their performance w.r.t AP in BEV on the DAIR-V2X-I benchmark. Results in Table 7 show that directly using the predicted 2D boxes (with predicted class labels) as prompts performs better.

Table 8: Inference time and parameters between our BEVPrompt and BEVHeight. We use two different 2D detectors in our BEVPrompt, namely YOLOV7 and DINO. We list the number of parameters of 3D detector plus 2D detector. Briefly, our model BEVPrompt “w/ YOLOV7” boosts 3D detection performance by 5.9 AP over the prior art BEVHeight, with faster inference speed (15.4 vs. 13.0 FPS) and fewer parameters (86.6M vs. 94.7M)!

Methods	AP in BEV	#param. in million	wall-clock time (ms)	FPS
BEVHeight [55]	37.9	94.7	77	13.0
+ BEVPrompt w/ YOLOV7	43.8	82.1+4.5	65	15.4
+ BEVPrompt w/ DINO	47.0	82.1+21.2	73	13.7

Latency and parameters. Recall that our BEVPrompt achieves the best performance by using separate 2D and 3D detectors without sharing the visual encoder (Table 4). We study this model in Table 8 w.r.t model parameters, and the wall-clock time and FPS in processing a single RGB frame. Here, we run the 2D detector (either YOLOV7 or DINO) and the 3D detector encoder in parallel. Note that our BEVPrompt does not require an FPN for proposal detection and replaces ResNet18 BEV encoder with a single convolutional layer (Sec. 4.1). These changes make our BEVPrompt faster than the original BEVHeight in inference and hence higher FPS, regardless of exploiting either YOLOV7 [45] or DINO [55]. As a result, our model BEVPrompt “w/ YOLOV7” boosts 3D detection performance by 5.9 AP over the prior art BEVHeight, with faster inference speed (15.4 vs. 13.0 FPS) and fewer parameters (86.6M vs. 94.7M).

4.4 Societal Impacts and Limitations

Societal impacts. While our method achieves significantly better performance than prior works on the benchmark datasets of roadside 3D object detection, we note potential risks if directly using our method for vehicle-vehicle communication and vehicle-infrastructure cooperative perception. Real-world applications should treat our approach as a module and evaluate the whole system for ultimate goals. Methods developed with existing datasets might be biased towards specific cities and countries. For example, in some countries, vehicles are running on the different side of the road from what are presented in the datasets. These are potentially negative societal impacts.

Limitations. Our method outputs a 3D prediction for every 2D detection prompt. As 2D detections can be false positives, doing so inevitably hallucinates 3D detections which certainly are incorrect. While hallucination can be mitigated by training better 2D detectors towards better 3D detection (cf. Fig. 5), we expect future research to build upon our exploration to better solve the problem of roadside monocular 3D detection.

5 Conclusion

We address the problem of roadside monocular 3D detection and propose a novel framework which leverages a well-trained 2D detector to improve the training of the 3D detector. Particularly, our method uses 2D detections $\{x, y, \text{width}, \text{height}, \text{label}\}$ by the 2D detector as prompts, encodes them as features to fuse with 3D detector’s features, and decodes the fused features towards 3D detections. We validate our method through comprehensive experiments. Results show that our method significantly outperforms prior arts on publicly available benchmarks.

References

1. Arnold, E., Dianati, M., de Temple, R., Fallah, S.: Cooperative perception for 3d object detection in driving scenarios using infrastructure sensors. *IEEE Transactions on Intelligent Transportation Systems* **23**(3), 1852–1864 (2020) [1](#)
2. Bar, A., Gandelsman, Y., Darrell, T., Globerson, A., Efros, A.: Visual prompting via image inpainting. *Advances in Neural Information Processing Systems* (2022) [4](#)
3. Bochkovskiy, A., Wang, C.Y., Liao, H.Y.M.: Yolov4: Optimal speed and accuracy of object detection. *arXiv:2004.10934* (2020) [6](#)
4. Brazil, G., Liu, X.: M3d-rpn: Monocular 3d region proposal network for object detection. In: *Proceedings of the IEEE/CVF International Conference on Computer Vision*. pp. 9287–9296 (2019) [10](#)
5. Brazil, G., Pons-Moll, G., Liu, X., Schiele, B.: Kinematic 3d object detection in monocular video. In: *European Conference on Computer Vision* (2020) [10](#)
6. Brown, T., Mann, B., Ryder, N., Subbiah, M., Kaplan, J.D., Dhariwal, P., Neelakantan, A., Shyam, P., Sastry, G., Askell, A., et al.: Language models are few-shot learners. *Advances in neural information processing systems* **33**, 1877–1901 (2020) [4](#)
7. Caesar, H., Bankiti, V., Lang, A.H., Vora, S., Liong, V.E., Xu, Q., Krishnan, A., Pan, Y., Baldan, G., Beijbom, O.: nuscenes: A multimodal dataset for autonomous driving. In: *CVPR* (2020) [7, 11, 22, 23](#)
8. Carion, N., Massa, F., Synnaeve, G., Usunier, N., Kirillov, A., Zagoruyko, S.: End-to-end object detection with transformers. In: *ECCV* (2020) [4](#)
9. Carion, N., Massa, F., Synnaeve, G., Usunier, N., Kirillov, A., Zagoruyko, S.: End-to-end object detection with transformers. In: *European Conference on Computer Vision (ECCV)* (2020) [6](#)
10. Chen, Q., Tang, S., Yang, Q., Fu, S.: Cooper: Cooperative perception for connected autonomous vehicles based on 3d point clouds. In: *IEEE International Conference on Distributed Computing Systems (ICDCS)* (2019) [1](#)
11. Felzenszwalb, P.F., Girshick, R.B., McAllester, D., Ramanan, D.: Object detection with discriminatively trained part-based models. *IEEE transactions on pattern analysis and machine intelligence* **32**(9), 1627–1645 (2009) [4](#)
12. Geiger, A., Lenz, P., Urtasun, R.: Are we ready for autonomous driving? the kitti vision benchmark suite. In: *2012 IEEE conference on computer vision and pattern recognition*. pp. 3354–3361. IEEE (2012) [9](#)
13. Guo, X., Shi, S., Wang, X., Li, H.: Liga-stereo: Learning lidar geometry aware representations for stereo-based 3d detector. In: *Proceedings of the IEEE/CVF International Conference on Computer Vision*. pp. 3153–3163 (2021) [4](#)
14. Gupta, S., Kanjani, J., Li, M., Ferroni, F., Hays, J., Ramanan, D., Kong, S.: Far3det: Towards far-field 3d detection. In: *Proceedings of the IEEE/CVF Winter Conference on Applications of Computer Vision* (2023) [1, 3](#)
15. He, K., Zhang, X., Ren, S., Sun, J.: Deep residual learning for image recognition. In: *CVPR* (2016) [9, 22, 23](#)
16. Hu, Y., Yang, J., Chen, L., Li, K., Sima, C., Zhu, X., Chai, S., Du, S., Lin, T., Wang, W., Lu, L., Jia, X., Liu, Q., Dai, J., Qiao, Y., Li, H.: Planning-oriented autonomous driving. In: *Proceedings of the IEEE/CVF Conference on Computer Vision and Pattern Recognition* (2023) [4](#)
17. Kirillov, A., Mintun, E., Ravi, N., Mao, H., Rolland, C., Gustafson, L., Xiao, T., Whitehead, S., Berg, A.C., Lo, W.Y., et al.: Segment anything. *arXiv:2304.02643* (2023) [4, 6](#)
18. Lang, A.H., Vora, S., Caesar, H., Zhou, L., Yang, J., Beijbom, O.: Pointpillars: Fast encoders for object detection from point clouds. In: *IEEE Conference on Computer Vision and Pattern Recognition (CVPR)* (2019) [9](#)

19. Li, Y., Ma, D., An, Z., Wang, Z., Zhong, Y., Chen, S., Feng, C.: V2x-sim: Multi-agent collaborative perception dataset and benchmark for autonomous driving. *IEEE Robotics and Automation Letters* **7**(4), 10914–10921 (2022) [1](#)
20. Li, Y., Ge, Z., Yu, G., Yang, J., Wang, Z., Shi, Y., Sun, J., Li, Z.: Bevdepth: Acquisition of reliable depth for multi-view 3d object detection. In: *AAAI* (2023) [1](#), [4](#), [9](#), [10](#), [11](#), [22](#), [23](#)
21. Li, Z., Wang, W., Li, H., Xie, E., Sima, C., Lu, T., Qiao, Y., Dai, J.: Bevformer: Learning bird's-eye-view representation from multi-camera images via spatiotemporal transformers. In: *European Conference on Computer Vision* (2022) [1](#), [9](#), [10](#)
22. Lin, T.Y., Maire, M., Belongie, S.J., Hays, J., Perona, P., Ramanan, D., Dollár, P., Zitnick, C.L.: Microsoft coco: Common objects in context. In: *ECCV* (2014) [4](#)
23. Lin, T., Maire, M., Belongie, S.J., Hays, J., Perona, P., Ramanan, D., Dollár, P., Zitnick, C.L.: Microsoft COCO: common objects in context. In: *European Conference on Computer Vision (ECCV)* (2014) [7](#), [9](#)
24. Liu, H., Teng, Y., Lu, T., Wang, H., Wang, L.: Sparsebev: High-performance sparse 3d object detection from multi-camera videos. In: *Proceedings of the IEEE/CVF International Conference on Computer Vision*. pp. 18580–18590 (2023) [9](#), [10](#)
25. Liu, W., Anguelov, D., Erhan, D., Szegedy, C., Reed, S., Fu, C.Y., Berg, A.C.: Ssd: Single shot multibox detector. In: *ECCV* (2016) [4](#)
26. Liu, W., Shen, X., Pun, C.M., Cun, X.: Explicit visual prompting for low-level structure segmentations. In: *Proceedings of the IEEE/CVF Conference on Computer Vision and Pattern Recognition* (2023) [4](#)
27. Liu, X., Xue, N., Wu, T.: Learning auxiliary monocular contexts helps monocular 3d object detection. In: *Proceedings of the AAAI Conference on Artificial Intelligence*. vol. 36, pp. 1810–1818 (2022) [4](#)
28. Long, J., Shelhamer, E., Darrell, T.: Fully convolutional networks for semantic segmentation. In: *Proceedings of the IEEE conference on computer vision and pattern recognition*. pp. 3431–3440 (2015) [6](#)
29. Loshchilov, I., Hutter, F.: Decoupled weight decay regularization. In: *ICLR* (2019) [10](#)
30. Luo, Y., Zheng, C., Yan, X., Kun, T., Zheng, C., Cui, S., Li, Z.: Latr: 3d lane detection from monocular images with transformer. In: *Proceedings of the IEEE/CVF International Conference on Computer Vision*. pp. 7941–7952 (2023) [4](#)
31. Ma, X., Zhang, Y., Xu, D., Zhou, D., Yi, S., Li, H., Ouyang, W.: Delving into localization errors for monocular 3d object detection. In: *Proceedings of the IEEE/CVF Conference on Computer Vision and Pattern Recognition* (2021) [10](#)
32. Nichol, A., Dhariwal, P., Ramesh, A., Shyam, P., Mishkin, P., McGrew, B., Sutskever, I., Chen, M.: Glide: Towards photorealistic image generation and editing with text-guided diffusion models. *JMLR* (2021) [4](#)
33. Park, D., Ambrus, R., Guizilini, V., Li, J., Gaidon, A.: Is pseudo-lidar needed for monocular 3d object detection? In: *Proceedings of the IEEE/CVF International Conference on Computer Vision*. pp. 3142–3152 (2021) [4](#)
34. Pinheiro, P.O., Lin, T.Y., Collobert, R., Dollár, P.: Learning to refine object segments. In: *European conference on computer vision*. pp. 75–91. Springer (2016) [6](#)
35. Ramesh, A., Pavlov, M., Goh, G., Gray, S., Voss, C., Radford, A., Chen, M., Sutskever, I.: Zero-shot text-to-image generation. In: *International Conference on Machine Learning*. pp. 8821–8831. *PMLR* (2021) [4](#)
36. Rauch, A., Klanner, F., Rasshofer, R., Dietmayer, K.: Car2x-based perception in a high-level fusion architecture for cooperative perception systems. In: *IEEE Intelligent Vehicles Symposium*. pp. 270–275. *IEEE* (2012) [1](#)
37. Redmon, J., Divvala, S., Girshick, R., Farhadi, A.: You only look once: Unified, real-time object detection. In: *Proceedings of the IEEE conference on computer vision and pattern recognition*. pp. 779–788 (2016) [4](#)

38. Ren, S., He, K., Girshick, R., Sun, J.: Faster r-cnn: Towards real-time object detection with region proposal networks. In: Advances in Neural Information Processing Systems (2015) 4, 6

39. Rukhovich, D., Vorontsova, A., Konushin, A.: Imvoxelnet: Image to voxels projection for monocular and multi-view general-purpose 3d object detection. In: Proceedings of the IEEE/CVF Winter Conference on Applications of Computer Vision. pp. 2397–2406 (2022) 9

40. Rushton, S.K., Duke, P.A.: Observers cannot accurately estimate the speed of an approaching object in flight. *Vision research* **49**(15), 1919–1928 (2009) 1

41. Sanh, V., Webson, A., Raffel, C., Bach, S.H., Sutawika, L., Alyafeai, Z., Chaffin, A., Stiegler, A., Scao, T.L., Raja, A., et al.: Multitask prompted training enables zero-shot task generalization. In: ICLR (2022) 4

42. Simonelli, A., Bulo, S.R., Porzi, L., López-Antequera, M., Kuntschner, P.: Disentangling monocular 3d object detection. In: Proceedings of the IEEE/CVF International Conference on Computer Vision. pp. 1991–1999 (2019) 4, 9

43. Sindagi, V.A., Zhou, Y., Tuzel, O.: Mvx-net: Multimodal voxelnet for 3d object detection. In: International Conference on Robotics and Automation (ICRA) (2019) 9

44. Vaswani, A., Shazeer, N., Parmar, N., Uszkoreit, J., Jones, L., Gomez, A.N., Kaiser, Ł., Polosukhin, I.: Attention is all you need. *Advances in neural information processing systems* **30** (2017) 6

45. Wang, C.Y., Bochkovskiy, A., Liao, H.Y.M.: Yolov7: Trainable bag-of-freebies sets new state-of-the-art for real-time object detectors. *arXiv:2207.02696* (2022) 4, 6, 11, 14

46. Wang, T., Lian, Q., Zhu, C., Zhu, X., Zhang, W.: Mv-fcos3d++: Multi-view camera-only 4d object detection with pretrained monocular backbones. *arXiv preprint arXiv:2207.12716* (2022) 4

47. Wang, T., Zhu, X., Pang, J., Lin, D.: FCOS3D: fully convolutional one-stage monocular 3d object detection. In: ICCV (2021) 4

48. Wang, T.H., Manivasagam, S., Liang, M., Yang, B., Zeng, W., Urtasun, R.: V2vnet: Vehicle-to-vehicle communication for joint perception and prediction. In: European Conference on Computer Vision (2020) 1

49. Wang, X., Wang, W., Cao, Y., Shen, C., Huang, T.: Images speak in images: A generalist painter for in-context visual learning. In: Proceedings of the IEEE/CVF Conference on Computer Vision and Pattern Recognition. pp. 6830–6839 (2023) 4

50. Wang, Z., Huang, Z., Fu, J., Wang, N., Liu, S.: Object as query: Lifting any 2d object detector to 3d detection. In: Proceedings of the IEEE/CVF International Conference on Computer Vision. pp. 3791–3800 (2023) 4, 9

51. Wei, J., Tay, Y., Bommasani, R., Raffel, C., Zoph, B., Borgeaud, S., Yogatama, D., Bosma, M., Zhou, D., Metzler, D., Chi, E.H., Hashimoto, T., Vinyals, O., Liang, P., Dean, J., Fedus, W.: Emergent abilities of large language models. *Transactions on Machine Learning Research* (2022) 4

52. Welchman, A.E., Tuck, V.L., Harris, J.M.: Human observers are biased in judging the angular approach of a projectile. *Vision research* **44**(17), 2027–2042 (2004) 1

53. Yan, Y., Mao, Y., Li, B.: Second: Sparsely embedded convolutional detection. *Sensors* **18**(10), 3337 (2018) 9

54. Yang, C., Chen, Y., Tian, H., Tao, C., Zhu, X., Zhang, Z., Huang, G., Li, H., Qiao, Y., Lu, L., et al.: Bevformer v2: Adapting modern image backbones to bird’s-eye-view recognition via perspective supervision. In: Proceedings of the IEEE/CVF Conference on Computer Vision and Pattern Recognition. pp. 17830–17839 (2023) 4, 9

55. Yang, L., Yu, K., Tang, T., Li, J., Yuan, K., Wang, L., Zhang, X., Chen, P.: Bevheight: A robust framework for vision-based roadside 3d object detection. In: CVPR (2023) 1, 2, 3, 8, 9, 10, 11, 13, 14, 20, 21, 22, 23

56. Ye, X., Shu, M., Li, H., Shi, Y., Li, Y., Wang, G., Tan, X., Ding, E.: Rope3d: The roadside perception dataset for autonomous driving and monocular 3d object detection task. In: Proceedings of the IEEE/CVF Conference on Computer Vision and Pattern Recognition. pp. 21341–21350 (2022) [1](#), [3](#), [8](#), [9](#), [10](#)
57. Yin, T., Zhou, X., Krahenbuhl, P.: Center-based 3d object detection and tracking. In: CVPR (2021) [8](#)
58. Yu, H., Luo, Y., Shu, M., Huo, Y., Yang, Z., Shi, Y., Guo, Z., Li, H., Hu, X., Yuan, J., et al.: Dair-v2x: A large-scale dataset for vehicle-infrastructure cooperative 3d object detection. In: CVPR (2022) [1](#), [2](#), [3](#), [8](#), [19](#), [22](#)
59. Zhang, H., Li, F., Liu, S., Zhang, L., Su, H., Zhu, J., Ni, L., Shum, H.: Dino: Detr with improved denoising anchor boxes for end-to-end object detection. In: International Conference on Learning Representations (2022) [2](#), [4](#), [6](#), [10](#), [11](#)
60. Zhang, Y., Lu, J., Zhou, J.: Objects are different: Flexible monocular 3d object detection. In: Proceedings of the IEEE/CVF Conference on Computer Vision and Pattern Recognition. pp. 3289–3298 (2021) [4](#), [10](#)
61. Zhu, B., Jiang, Z., Zhou, X., Li, Z., Yu, G.: Class-balanced grouping and sampling for point cloud 3d object detection. arXiv preprint arXiv:1908.09492 (2019) [7](#)
62. Zhu, X., Su, W., Lu, L., Li, B., Wang, X., Dai, J.: Deformable detr: Deformable transformers for end-to-end object detection. arXiv:2010.04159 (2020) [4](#)

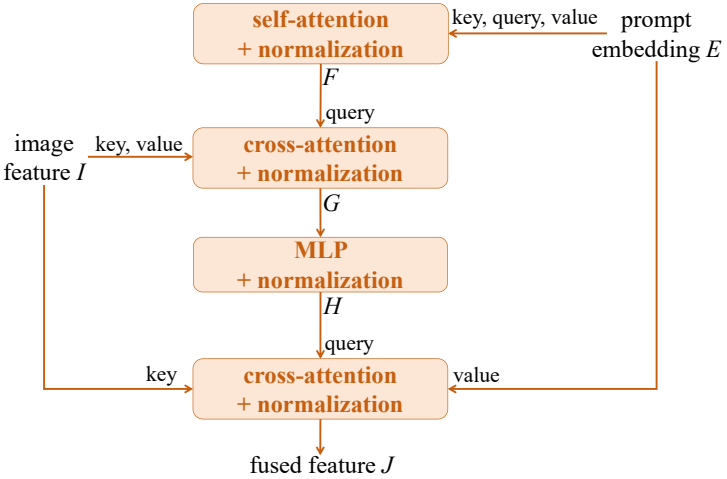


Fig. 8: Illustration of our proposed fusion module, which takes the feature prompts E from 2D detector and image feature I from 3D detector as input and finally outputs the fused feature J .

A The Architecture of BEVPrompt

In this section, we describe the architecture of BEVPrompt which uses 2D detection outputs as prompts.

Prompt encoder transforms the 2D detection outputs to features through three consecutive steps: (1) normalizing the top-left and bottom-right coordinates of a 2D detection box, denoted as $A \in \mathbb{R}^{2 \times 2}$; (2) multiplying A by a random matrix $B \in \mathbb{R}^{2 \times 512}$ whose entries are initialized using a Gaussian distribution, and then add a learnable matrix $C \in \mathbb{R}^{2 \times 512}$ to get $D = A \times B + C$; (3) repeating the predicted class label (represented as an unique class ID) 512 times to get a 512-dimensional vector, and concatenating it with D to obtain the final feature prompts $E \in \mathbb{R}^{3 \times 512}$.

Fusion module aims to fuse the feature prompts E with the feature map I of the 3D detector’s encoder. We use a transformer module to fuse these two features, as shown in Fig. 8. It has four computation steps: (1) applying self-attention on the feature prompts E and then normalize it to obtain F ; (2) applying cross-attention to F and then normalize it to obtain G , where the key and value of the cross-attention are the image feature I , and the query is F ; (3) updating G through point-wise MLP and normalize it to obtain H ; (4) applying cross-attention to H and normalize it to obtain the final output J .

B Ablation Study on Class Grouping

While data are oftentimes labeled with a vocabulary of fine-grained classes, real-world applications might not require distinguishing some fine-classes but consider them as a whole. For example, the DAIR-V2X-I dataset [58] annotates images w.r.t {truck,

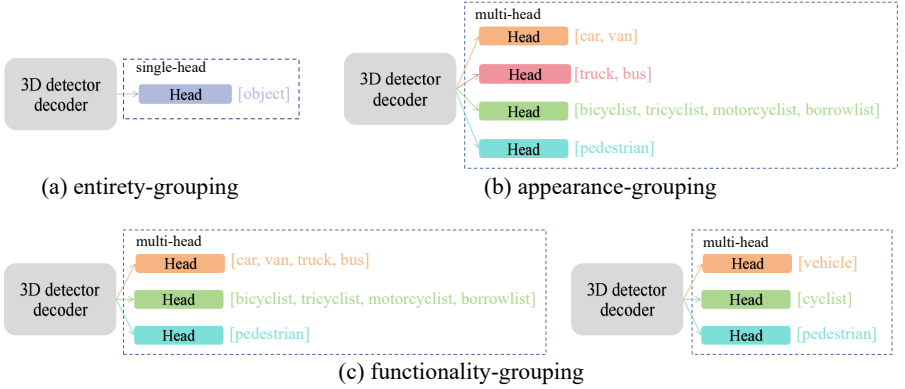


Fig. 9: Illustration of different grouping strategies and detector head designs. We study three grouping strategies in this supplement, i.e., entirety-based grouping, appearance-based grouping and functionality-based grouping. (a) merges all the classes into a single super-class “object” and predicts specific labels by the 2D detector. (b) groups classes according to their appearance similarity and uses multi-head for prediction. (c) groups classes according to their functionalities and employs multi-head for prediction, where each head could be a fine-grained class predictor (left) or a single super-class predictor (right).

bus, car, van, bicyclist, tricyclist, motorcyclist, barrowlist, pedestrian}, but its evaluation protocol reports numbers on superclasses of {vehicle, cyclist, pedestrian}, where vehicle={truck, bus, car, van}, and cyclist={bicyclist, tricyclist, motorcyclist, barrowlist}.

On the other hand, to facilitate training, a common practice is to group fine-grained classes into superclasses and train superclass-specific heads, each of which makes predictions only within the specific superclass. Class grouping is oftentimes based on object appearance. For example, BEVHeight [55] adopts an appearance-based grouping strategy, creating three superclasses that merge {truck, bus}, {car, van}, and {bicyclist, tricyclist, motorcyclist, barrowlist}, respectively, along with the origin *pedestrian* class. As we can see, both *truck* and *bus* are big vehicles so they are grouped together. Based on such superclasses, BEVHeight [55] learns a four-head detector.

In this paper, we suggest a functionality-based grouping strategy, motivated by the fact that vehicles, cyclists and pedestrians appear at relatively fixed regions in the image. For each 3D detector head, we can train it using a single superclass label (a.k.a. 1-way classifier) or multiple fine-class labels (a.k.a. K -way classifier) shown in Fig. 9c. We carry out comprehensive analysis on how these grouping strategies affect the final roadside 3D detection performance.

In this supplement, we combine all these different classes grouping and multi-head designs in 3D detector, shown in Fig. 9, and evaluate them on the DAIR-V2X-I dataset. Note that 2D detectors can also adopt class grouping, we can train it using superclass labels or multiple fine-class labels. Table 9 lists quantitative comparisons. We summarize key observations below.

Table 9: Results of different class-grouping strategies and detector-head designs. For entirety-based grouping, we merge all classes into a single super-class, and use the predicted labels from the 2D detector as the final labels for 3D detection. For functionality-based grouping, we study training with fine-classes vs. a super-class in a head (cf. Fig.9c), where the latter yields the best results.

Method	Vehicle			Cyclist			Pedestrian		
	Easy	Mid	Hard	Easy	Mid	Hard	Easy	Mid	Hard
BEVHeight [55] w/ appearance-grouping, multi-head (default)	67.4	67.2	67.2	23.6	25.9	26.5	11.5	11.4	11.5
BEVHeight [55] w/ functionality-grouping, multi-head (ours)	72.0	73.6	72.0	23.5	25.7	26.4	10.1	10.1	10.2
BEVPrompt w/ entirety-grouping, single-head, 1-way cls	74.1	74.0	73.0	31.1	35.7	35.3	14.4	14.3	14.4
+ DINO w/ super-class cls									
BEVPrompt w/ entirety-grouping, single-head, 1-way cls	73.8	74.3	73.1	31.0	35.6	35.3	14.3	14.3	14.3
+ DINO w/ fine-class cls									
BEVPrompt w/ appearance-grouping, multi-head, K -way cls	74.0	74.4	73.3	32.0	35.9	35.6	17.7	17.7	17.7
+ DINO w/ super-class cls									
BEVPrompt w/ appearance-grouping, multi-head, K -way cls	73.7	74.6	73.3	31.8	36.0	35.4	17.8	17.6	17.7
+ DINO w/ fine-class cls									
BEVPrompt w/ functionality-grouping, multi-head, K -way cls	74.4	76.0	73.9	31.9	36.1	35.8	17.6	17.7	17.5
+ DINO w/ super-class cls									
BEVPrompt w/ functionality-grouping, multi-head, K -way cls	74.2	75.9	73.9	31.8	35.9	35.6	17.5	17.5	17.6
+ DINO w/ fine-class cls									
BEVPrompt w/ functionality-grouping, multi-head, 1-way cls	75.3	77.2	74.5	32.1	36.1	36.0	17.8	17.7	17.7
+ DINO w/ super-class cls									
BEVPrompt w/ functionality-grouping, multi-head, 1-way cls	75.1	77.0	74.7	32.0	35.9	36.0	17.7	17.6	17.6
+ DINO w/ fine-class cls									

Table 10: Results of occluded and truncated obstacles. We split occlusions and truncations with different ranges (0%~50% and 50%~100%), respectively. Our approach BEVPrompt resoundingly outperforms BEVHeight [55] on all the three superclasses in each range.

(a) Occlusion of 0%~50%				(b) Occlusion of 50%~100%			
Methods	Vehicle	Cyclist	Pedestrian	Methods	Vehicle	Cyclist	Pedestrian
BEVHeight [55]	37.6	6.9	3.7	BEVHeight [55]	35.7	2.9	0.9
+ BEVPrompt	46.7	12.0	6.7	+ BEVPrompt	45.2	8.2	3.5
(c) Truncation of 0%~50%				(d) Truncation of 50%~100%			
Methods	Vehicle	Cyclist	Pedestrian	Methods	Vehicle	Cyclist	Pedestrian
BEVHeight [55]	57.9	23.0	3.2	BEVHeight [55]	0.5	1.2	0.1
+ BEVPrompt	69.2	29.8	9.2	+ BEVPrompt	1.5	2.8	1.6

- Comparison between the first two rows in Table 9 shows that functionality-grouping yields much better performance than appearance-based grouping (i.e., the default strategy in BEVHeight [55]) on the vehicle class.
- Comparison within the 2nd or 3rd row-panel shows that training fine-classes or super-classes in the 2D detector does not make a big difference on the final 3D detection performance. This suggests that 2D detectors is quite robust to different grouping configurations.
- Comparing the 2nd with the 3rd row-panel, we see that multi-head 3D detector plus K -way classifier (i.e., each head makes K -way classification on its fine-grained classes) performs much better than single-head design — the former achieves 17.7 AP whereas the latter achieves 14.3 AP for *pedestrian* class.
- Within the last row-panel, we see that with functionality-based grouping, training a multi-head 3D detector using superclass labels only is better than using fine-grained class labels (i.e., more fine-grained class labels within each superclass for each detector head).

C Results under Occlusion and Truncation

Objects might be occluded by others or truncated around the image borders. We carry out breakdown analysis on how detectors perform in these scenarios. The DAIR-V2X-I dataset provides occlusion and truncation tags. Following [58], we split occlusions and truncations with 0%~50% and 50%~100% for different superclasses, respectively. As shown in Table 10, our method gets better APs on the all superclasses in different ranges of occlusions and truncations. This shows that our method BEVPrompt is more robust than BEVHeight [55].

D Robustness to Noises of Camera Pose

We consider the robustness of BEVPrompt to noises in camera calibration parameters. We follow BEVHeight [55] to add noises on camera pitch and roll. Table 11 compares the robustness of BEVDepth [20], BEVHeight [55] and our BEVPrompt. Clearly, BEVPrompt is more robust than prior works to camera noise.

Table 11: Robustness to camera noise. We follow BEVHeight [55] to simulate calibration errors by adding noises to camera pitch and roll. Results show that BEVprompt is more robust than BEVHeight [55] and BEVDepth [20] to these camera pose noises.

Method	Vehicle			Cyclist			Pedestrian		
	Easy	Mid	Hard	Easy	Mid	Hard	Easy	Mid	Hard
BEVDepth [20] + noise	64.1 8.9(-55.2)	64.0 9.0(-55.0)	64.0 9.4(-54.6)	20.9 3.3(-17.6)	21.5 3.9(-17.6)	22.7 4.0(-18.7)	10.1 1.8(-8.3)	10.2 1.5(-8.7)	10.1 1.5(-8.6)
BEVHeight [55] + noise	67.4 52.1(-15.3)	67.2 51.3(-15.9)	67.2 52.0(-15.2)	23.6 8.8(-14.8)	25.9 9.2(-16.7)	26.5 9.8(-16.7)	11.5 4.8(-6.7)	11.4 4.7(-6.7)	11.5 4.7(-6.8)
BEVPrompt + noise	75.9 63.8(-12.1)	77.6 64.8(-12.8)	77.3 65.4(-11.9)	34.1 21.4(-12.7)	36.1 24.9(-11.2)	36.0 26.0(-10.0)	18.9 12.7(-6.2)	18.6 12.3(-6.3)	18.5 12.2(-6.3)

E Results on nuScenes dataset

We further study BEVPrompt on the well-established ego-vehicle nuScenes dataset [7] in this supplement. We follow the suggested protocol in [20], using 10 standard categories for comparison. As shown in Table 12, where all methods use ResNet-50 backbone [15] and the resolution of input image is 864x1536 following [55], BEVPrompt still significantly outperforms BEVDepth [20] and BEVHeight [55].

F More Visualizations

Figure 10 visualizes more results on the DAIR-V2X-I dataset [58]. BEVPrompt not only has better orientation predictions for vehicles but also can detect hard objects such as infrequently-seen ambulances, occluded pedestrians and cyclists. We provide a video of our results in the supplement.

Table 12: Results on nuScenes validation dataset. We apply BEVPrompt to BEVDepth [20] and BEVHeight [55] methods on ego-vehicle dataset nuScenes [7]. Results show that our BEVPrompt still outperforms these competitors. Note that all the methods use the ResNet-50 backbone [15] and the resolution of input image is 864*1536 following [55].

	mAP↑	NDS↑	mATE↓	mASE↓	mAOE↓	mAVE↓	mAAE↓
BEVDepth [20]	0.315	0.367	0.702	0.271	0.621	1.042	0.315
BEVDepth*	0.312	0.355	0.710	0.275	0.658	1.135	0.379
+ BEVPrompt	0.337	0.388	0.682	0.254	0.590	0.992	0.284
BEVHeight [55]	0.291	0.342	0.722	0.278	0.674	1.230	0.361
BEVHeight*	0.298	0.349	0.719	0.276	0.668	1.138	0.350
+ BEVPrompt	0.329	0.380	0.694	0.267	0.598	1.001	0.296

* denotes the results we reproduce.

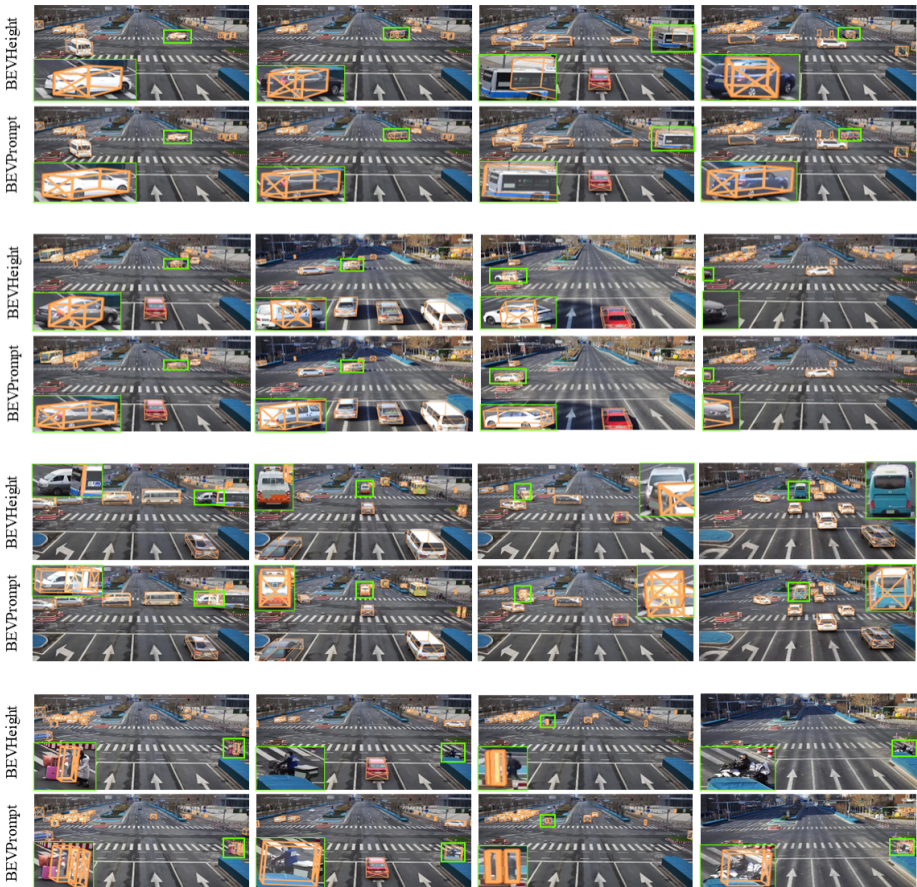


Fig. 10: More visualizations between the state-of-the-art method BEVHeight [55] and our BEVPrompt.